2020 IEEE/RSJ International Conference on Intelligent Robots and Systems (IROS)
October 25-29, 2020, Las Vegas, NV, USA (Virtual)

Expert-Emulating Excavation Trajectory Planning for Autonomous Robotic Industrial Excavator

Bukun Son[1], ChangU Kim[1], Changmuk Kim[1,2], Dongjun Lee[1]

***Abstract*— We propose a novel excavation (i.e., digging) trajectory planning framework for industrial autonomous robotic excavators, which emulates the strategies of human expert operators to optimize the excavation of (complex/unmodellable) soils while also upholding robustness and safety in practice. First, we encode the trajectory with dynamic movement primitives (DMP), which is known to robustly preserve qualitative shape of the trajectory and attraction to (variable) end-points (i.e., start-points of swing/dumping), while also being data-efficient due to its structure, thus, suitable for our purpose, where expert data collection is expensive. We further shape this DMP-based trajectory to be expert-emulating, by learning the shaping force of the DMP-dynamics from the real expert excavation data via a neural network (i.e., MLP (multi-layer perceptron)). To cope with (possibly dangerous) underground uncertainties (e.g., pipes, rocks), we also real-time modulate the expert-emulating (nominal) trajectory to prevent excessive build-up of excavation force by using the feedback of its online estimation. The proposed framework is then validated/demonstrated by using an industrial-scale autonomous robotic excavator, with the associated data also presented here.**

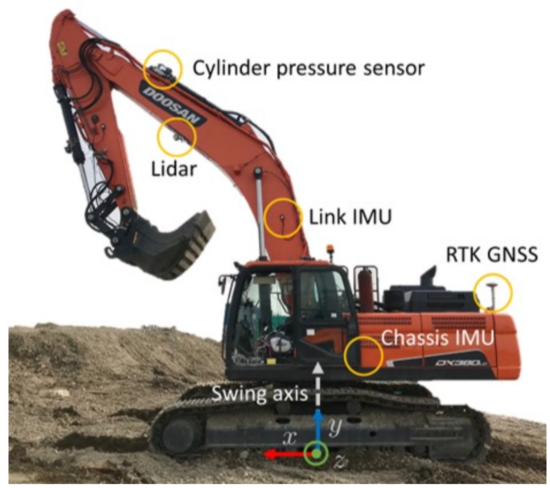

Fig. 1: Industrial autonomous robotic excavator, Doosan DX380LC, customized with IMUs, LiDAR, cylinder pressure sensor, RTK-GNSS sensors.

I. Introduction

Excavators are the mostly widely-used one among heavy machinery equipments at construction sites. Automation or robotization of these excavators have received great attention for a long time (e.g., [1]), since it can improve construction efficiency via over-the-clock operation while eliminating operator health, fatigue or safety concerns. It is becoming equally challenging to find a skilled operator for excavators, particularly in many fast-aging countries. With the advancements of sensors, computing, communication and actuators, the construction machinery industry now starts to embark on the commercialization of this autonomous (or automated) excavator, with some of its component technologies already commercialized or very close to that (e.g., machine control [2]–[4], machine guidance [5]).

In this paper, we focus on the excavation (i.e., soil digging) operation of the autonomous excavators. Achieving this autonomous excavation, while maximizing digging performance like an expert human operator, is challenging since soil dynamics is too complicated to be captured by a model compact enough to be useful for real-time control. Prior motion planning results for the autonomous excavator typically do not consider this soil dynamics and rather only focus on the kinematic control of the excavator with the soil-interaction dynamics not taken into account [6], [7]. Some works incorporate this soil dynamics into the motion planning, yet, only for simple straight line trajectory [8], certain fixed-shape trajectory [9], or simplified trajectory in three steps [10], [11], thus, not applicable to generate expert-like complicated excavation trajectory.

To overcome this challenge related to the complex/unmodellable soil dynamics, in this paper, we adopt the data-driven/learning technique. In particular, we aim to emulate the behavior of expert operators given the shape of the terrain. More precisely, as a human expert devises the (nominal) digging plan right after seeing the terrain, we develop a technique of expert-emulating trajectory planning as a function of geometric parameters (i.e., task parameters, in this paper) of the terrain. In particular, we adopt dynamic movement primitives (DMP, [12]), which utilizes a virtual dynamics to "structure" the trajectory and is known to preserve the qualitative shape of the trajectory and the attraction to the ending point (e.g., transition to swing/dump operation), thereby, substantially enhancing robustness and safety against operational/environmental variability in real practice while also providing high data-efficiency. We also endow this DMP-based trajectory with the ability of emulating expert human operators by learning the shaping force for this DMP-based trajectory from the expert excavation data with a neural network (MLP (multi-layer perceptron, [13])). Moreover, to address underground uncertainty (e.g.,

[1]Department of Mechanical & Aerospace Engineering and IAMD, Seoul National University, Seoul, South Korea. {sonbukun, kcu11, djlee}@snu.ac.kr,
[2]Doosan Infracoore, Seoul, South Koera. changmuk.kim@doosan.com
Research supported by Doosan Infracoore. Corresponding author: Dongjun Lee.

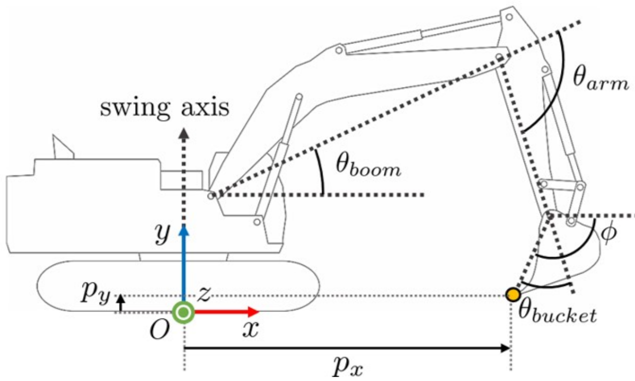

Fig. 2: Configuration of the industrial autonomous robotic excavator, Doosan DX380LC

pipes, rocks), we also add, on this DMP-based expert-emulating trajectory, the modulating force, which real-time adjusts the trajectory to prevent excessive excavation force build-up by feedbacking the estimate of excavation force. It is noteworthy to emphasize that our proposed framework, to be demonstrated with real machines [14], [15], where some unstable behaviors can result in costly damages to the machines or even in human casualty, is chosen with the robustness and safety as the foremost requirements, which we believe is utterly important for autonomous excavators, as, for them, no intervention by a (sensory-rich) on-board human operator is possible whatsoever. This also directs us to choose the techniques of DMP and MLP instead of more advanced/recent schemes, as they are known to be robust and well-behaving in many real applications. The results of this paper have been successfully demonstrated using real construction machines [14], [15]. To our knowledge, this current paper proposes the very first result of expert-emulating trajectory planning and its real demonstration with an industrial-scale autonomous robotic excavator.

The rest of the paper is organized as follows. System description and some preliminary materials about DMP and force estimation are introduced in Sec. II. Nominal excavation trajectory learning from the expert operation data is proposed in Sec. III, and its online modulation with the real-time excavation force feedback explained in Sec. IV. Experimental results to validate our proposed algorithm are presented in Sec. V, followed by some concluding remarks in Sec. VI.

II. PRELIMINARY

A. System Description

The autonomous robotic industrial excavator, we consider in this paper, is the commercial Doosan DX380LC as shown Fig. 1, which is customized with additional actuator (i.e., motors directly commanding the joystick to control the MCV (main control valve [16]) and sensors (i.e., IMU (inertial measurement unit) attached at each boom, arm and bucket links to measure their angle, cylinder pressure sensors, and RTK-GNSS (real-time kinetic global navigation satellite systems) to measure the pose of the cabin, and a Velodyne Puck VLP-16 LiDAR (light detection and ranging) sensor to scan the terrain to excavate). See Fig. 2.

In this paper, we assume the excavator motion is only within its sagittal plane, since, during the excavation, which is the focus of this paper, the swing motion is typically not involved. Further, here, we only consider the problem of expert-emulating trajectory planning with the low-level joint angle control already taken care of by manufacturer-provided PI (proportional-integral) control with IMU-feedback. The motion of the excavator can then be specified by $\theta = (\theta_{boom}, \theta_{arm}, \theta_{bucket}) \in \mathbb{R}^3$, which defines a configuration of the excavator in the sagittal plane (i.e., $SE(2)$). Another configuration can be defined to be $q = (p_x, p_y, \phi) \in SE(2)$, where p_x and p_y are the position and ϕ is the orientation of bucket tip related to the inertia frame O, whose origin is located at the floor-center of the excavator - see Fig. 2. With no redundancy, we then have one-to-one mapping between $\theta \in \mathbb{R}^3$ and $q \in SE(2)$. In the following, we will mostly utilize $q \in SE(2)$, while $\theta \in \mathbb{R}^3$ only for the real-time excavation force estimation.

B. Dynamic Movement Primitives (DMP)

DMP is widely used for learning and representing movements in robotics [12] [17]. It expresses a trajectory as a nonlinear external force applied to the unit mass critically-damped system. In this paper, we assign scalar DMP dynamics to each of p_x, p_y, both of which share the common clock signal $s \in [0, 1]$ with the following dynamics.

$$\tau \dot{s} = -\alpha_s s \tag{1}$$

where $\tau > 0$ and $\alpha_s > 0$ are parameters defining the temporal scaling of s, and $s(0) = 1$. The scalar DMP dynamics for each p_x and p_y then has the following form:

$$\tau \ddot{y} = \alpha_y(\beta_y(y_g - y) - \dot{y}) + f(s) \tag{2}$$

$$f(s) = h(s)(y_g - y_0)s \tag{3}$$

where $y_0 \in \mathbb{R}$ is the initial point, $y_g \in \mathbb{R}$ is the goal point, α_y, $\beta_y > 0$ are the gains, and $f(s) \in \mathbb{R}$ is the *shaping force*, which consists of a nonlinear function $h(s) \in \mathbb{R}$ and spatial scaling factor $y_g - y_0$, with the goal-directed attraction guaranteed by multiplying a monotonically diminishing clock signal s. Here, we relate the DMP dynamics only to the behaviors of p_x and p_y, whereas that of ϕ determined by the geometric relation between the bucket tooth and the digging trajectory - see Sec. III-C. In this paper, we use DMP with the shaping force $f(s)$ to generate the (nominal) expert-emulating excavation trajectory - see Sec. III-B.

C. Coupling Movement Primitives

DMP allows for online modulation through an additional modulation force called the coupling term (or *modulation force*, in this paper). The naive way for this is to directly add a coupling forcing term into the acceleration levels of the DMP [18], which however is known to possibly induce overshoot behavior. To avoid this, the technique of coupling movement primitives is suggested to control the desired dynamics like a PD (proportional-derivative) controller by adding a coupling term to both the acceleration-level and velocity-level DMP dynamics [19]. In this paper, we use this technique by injecting the modulating force term C into the DMP dynamics (2) s.t.,

$$\tau\dot{z} = \alpha_y(\beta_y(y_g - y) - z) + f(s) + c_2\dot{C} \tag{4}$$

$$\tau\dot{y} = z + c_1 C \tag{5}$$

where c_1 and c_2 are constant gains - see [19] for more details on the coupling movement primitives. In this paper, we utilize this technique of coupling movement primitives to real-time adjust the nominal trajectory with the excavation force feedback - see Sec. IV.

D. Excavation Force Estimation

During excavation, it is possible to encounter with underground objects (pipes, rocks, etc.), which cannot be predicted only by visually observing the terrain. These objects, however, can pose significant perturbation to the autonomous excavator, and, consequently, danger to that. To avoid this, information about the excavation force is desired. To obtain this, the most straightforward option is to attach F/T (force/torque) sensor at the bucket joint, which is however considered not yet viable due to the reliability and cost concerns. Instead, in this paper, we utilize the momentum-based wrench estimator [11], [20] to real-time estimate the excavation force and adjust the nominal trajectory based on that information. More precisely, consider the dynamics of the excavator:

$$M(\theta)\ddot{\theta} + C(\theta,\dot{\theta})\dot{\theta} + g(\theta) + F_s\mathrm{sgn}(\dot{\theta}) + B\dot{\theta} = \tau_u + \tau_{ext} \tag{6}$$

where $\theta \in \mathbb{R}^3$ is the configuration of the excavator, $M(\theta) \in \mathbb{R}^{3\times3}$ is the positive-definite inertia matrix, $C(\theta,\dot{\theta}) \in \mathbb{R}^3$ is the centripetal Coriolis vector, $g(\theta) \in \mathbb{R}^3$ is the gravitational vector, $F_s \in \mathbb{R}^{3\times3}$ and $B \in \mathbb{R}^{3\times3}$ are the Coulomb and viscous friction matrices, and $\tau_u, \tau_{ext} \in \mathbb{R}^3$ are the control input and the excavation torque (to estimate), respectively.

Since the excavation speed is typically relatively slowly, we can estimate the excavation torque τ_{ext} using the momentum-based disturbance observer [20], which is given by

$$\tau_{ext} = K_0(p(t) - \int_0^t (\tau_u - \tau_\mu - \beta(\theta,\dot{\theta}) + \tau_{ext})ds - p(0)) \tag{7}$$

with the generalized momentum $p(t) = M(\theta)\dot{\theta}$, $\beta = g(\theta) - C^T(\theta,\dot{\theta})\dot{\theta}$ and, $\tau_\mu = F_s\mathrm{sgn}(\dot{\theta}) + B\dot{\theta}$. Note that (7) defines a first-order low-pass-filter equation for τ_{ext}, for which we can directly measure $\theta, \dot{\theta}$ with the IMUs and τ_u with the cylinder pressure sensors, whereas all the other terms can be identified via off-line parameter optimization. The excavation force $f_{ext} \in \mathbb{R}^3$ in the q-space can then be computed by $f_{ext} = J_{ext}^{-T}\tau_{ext}$, where $J_{ext} \in \mathbb{R}^{3\times3}$ is the Jacobian from the q-space to the θ-space, which is non-singular for the range of excavator motion.

III. Nominal Excavation Trajectory Planning with Expert Emulation

A. Task Parameters Extraction

We extract geometric features that represent the shape of the terrain (i.e., depth and slope), and use them as *task parameters* as the input to the nominal excavation trajectory planning. We choose to use these task parameters instead of applying end-to-end learning algorithms directly to the point cloud data (PCD) of the LiDAR sensor, since they typically require very large amount of data for learning [21].

For this, we extract geometric features from a separate feature extractor to learn with a small number of expert data. Considering the motion of the excavator, the range of interest (ROI) of the relevant PCD is defined to be 3$\sim$11m in the x-direction and -1.5$\sim$1.5m in the z-direction - see Fig. 2. We also assume the default terrain shape as the sloped terrain with a irregular pit, the most common in construction sites. Then, after flattening the PCD in the z-direction, the slope surface of the terrain is extracted by the following fitting operation in the (x, y)-plane:

$$\begin{aligned} y(x) = ax + b - aH(x_1 - x)(x - x_1) \\ - aH(x - x_2)(x_2 - x) \end{aligned} \tag{8}$$

where $H(w) := \frac{d}{dw}\max(w, 0)$ is the heaviside function, x_1, x_2 are the initial and end points of the slop, and a, b are the slope/offset parameters. We also fit the slope surface with

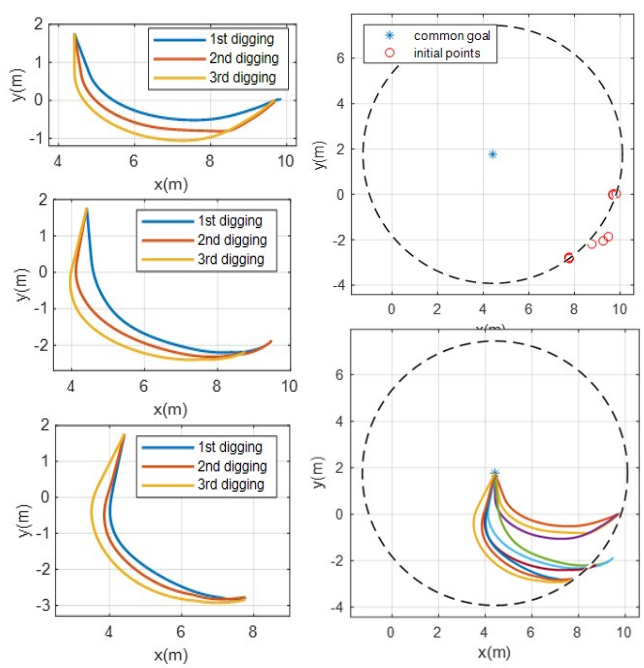

(a) (b)

Fig. 3: The acquired expert excavation trajectories (processed data from eighteen data-set): (a) three rounds of consecutive excavation in flat and two different angled slopes; (b) modified training trajectory matching goal position y_g to equalize spatial scaling.

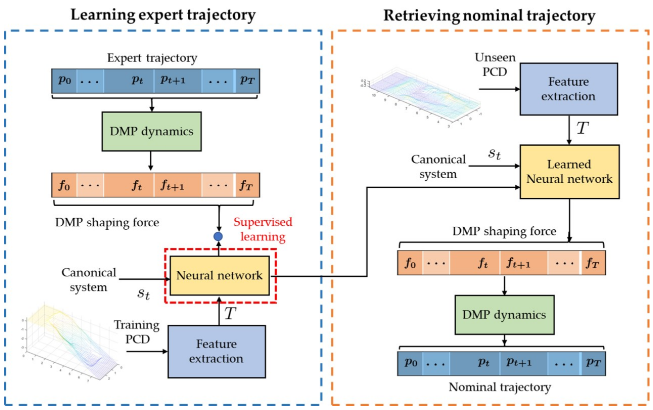

Fig. 4: An architecture of the learning and retrieving the nominal trajectory.

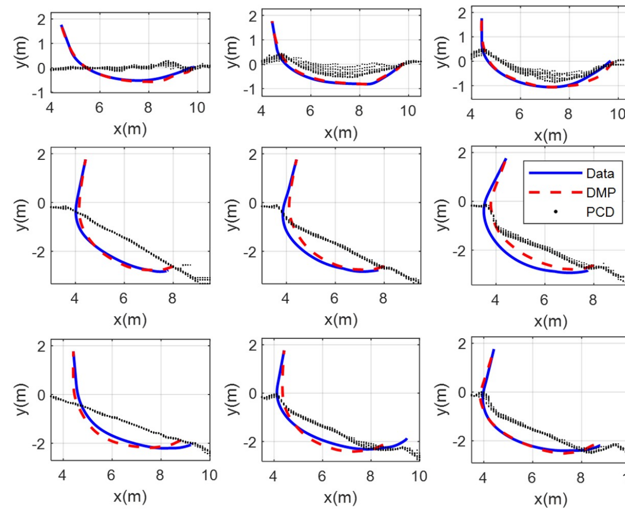

Fig. 5: Results of three times consecutive nominal trajectory retrieving in the training terrains from left to the right - top: flat terrain, middle: slope1, bottom: slope2

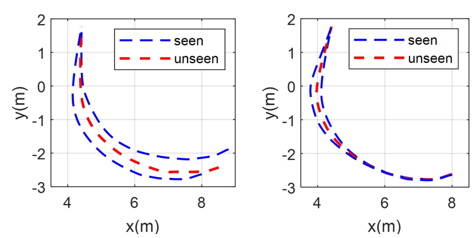

Fig. 6: Results of nominal trajectory retrieving for unseen test task parameters - left: test degree, right: test depth

the Gaussian function $d\exp(-(x-x_o)^2/c)$ to extract the depth parameter d and the deepest point x_o of the excavation terrain. We then choose the task parameters as the slope and the depth of the terrain, that is, $T = (\theta_{slope}, d) = (\tan^{-1}(a), d)$, which represent the terrain to excavate and serve as the input for the nominal expert-emulating excavation trajectory planning.

B. Learning Nominal Expert-Emulating Trajectory

The nominal expert-emulating excavation trajectory is produced by using the learning from demonstration based on the expert excavation trajectory data (each marked with its corresponding terrain task parameters). The expert trajectories are acquired in the flat terrain and also from the terrains with two different slopes (20.38 and 28.30 degrees) for two consecutive rounds of digging as shown in Fig. 3a, from which we can notice certain structured patterns. To learn this pattern of the expert excavation trajectories, we utilize DMP, whose high data-efficiency is well-suited for our purpose as obtaining expert data for excavation is expensive and the number of our data set is rather limited (i.e., two rounds $\times$ three slopes = total eighteen data set).

The acquired data was normalized to facilitate learning. Temporal scaling is equalized among the nominal trajectories, and the sampling is executed in 800 steps with 100Hz during 8 second-internal, the average working time of expert data. To equalize the spatial scaling, a common goal is deduced through optimization that minimizes the difference between Euclidean distances from each initial position $p_o \in \mathbb{R}^2$ to the goal position $p_g = (p_{g_x}, p_{g_y}) \in \mathbb{R}^2$ by

$$\begin{aligned} \min_{p_g, p_r} \quad & \sum_{i=1}^{n} \text{abs}(\|p_o - p_g\| - p_r) \\ \text{s.t.} \quad & x_l \leq p_{g_x} \leq x_u \\ & y_l \leq p_{g_y} \leq y_u \end{aligned} \tag{9}$$

where $p_r \in \mathbb{R}$ is the common distance between p_o (given from the data) and p_g, x_u and x_l are the upper and lower bound of p_{g_x}, and y_u and y_l are that of p_{g_y}. We learn the nonlinear term $h(s)$ in the shaping force $f(s)$ of (2)-(3) except the term $(y_g - y_o)$ and the clock signal s. Then, the objective of the learning is to find a mapping function $N : (s, T) \to h(s)$. There are a variety of regression standards for learning the nonlinear function $h(s)$, and we apply a supervised learning via neural network, MLP (multi-layer perceptron) consisted of two fully-connected layers with 64 and 16 nodes each, that is known to be robust among similar methods and can express the expert complicated/high-order excavation trajectory in complex soil with the multiple inputs.

The nominal trajectory generation of (p_x, p_y) for the training data are shown in Fig. 5. The trajectories are similar to that of the expert, suggesting proper leaning of the specific structured pattern of the expert trajectories of Fig. 3a. For each time-stamp, the RMS (root mean square) error for the position yields 0.51m, and the dominant reason for the error is that the initial position has an error of 0.42m. Moreover, to validate the generalization performance for the unseen terrain, the nominal trajectories for the test angle and depth interpolated from the training set were evaluated shown in Fig. 6.

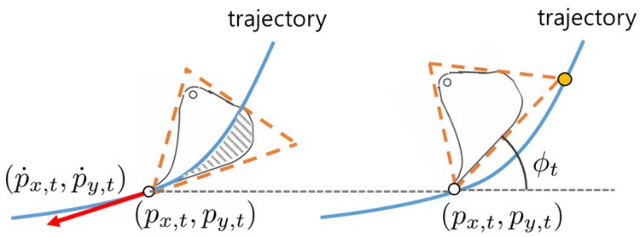

Fig. 7: Definition of bucket angle ϕ. (left) The bucket tooth and headings coincide but the bucket collide with the ground. (right) The bucket tooth and headings form the minimum angle avoiding collision.

C. Retrieving Nominal Trajectory

Now, note that the nominal DMP-based expert-emulating trajectory of Sec. III-B only specifies the motion for p_x, p_y, yet, the excavator possesses 3-DOF, thus, the redundancy occurs. To address this redundancy (to resolve $\phi(p_x, p_y)$), we devise a bucket angle algorithm as follows. First, notice from Fig. 7 that, if the bucket teeth simply align to the velocity vector of the trajectory, the shaded part of the bucket will collide or press against the ground in Fig. 7. To minimize such interaction force, a bucket angle ϕ is defined as the minimum angle between the bucket tooth and the trajectory velocity vector while the virtual triangle surrounding the bucket avoids the collisions as shown in Fig. 7. The algorithm contains the assumption that all soil in the trajectory passed is removed.

IV. Force-Based Online Trajectory Modulation

In this section, we acquire the excavation force data from the experts and propose an online trajectory modulation algorithm to prevent the excessive build-up of that excavation force. Since the nominal trajectory is the open-loop trajectory planning without considering interaction with the ground, problems can arise from unpredictable objects under the ground or various dynamic features of the terrain such as densities, shear strength, and flow velocity scale. The goal of the algorithm in this section is not to simply learn the expert's trajectory in position level but emulate the expert's force-based trajectory modulation technique, which is assumed to be optimal. We find out from the interview that the experts can recognize the external force on the bucket through the excavator movement in response to the joystick manipulation, and they modify the path in real-time if excessive force occurs. Therefore, we prevent excessive excavation force by acquiring the force patterns of experts and emulate them in real-time. In the previous force-based autonomous excavation studies, the force trajectory is defined by an engineer's intuition and is used for simplified trajectory and phase switching [10]. On the other hand, we have a remarkable difference in that we acquire the expert's contact force and generate a completely free-form trajectory planning rather than a limited and simplified one.

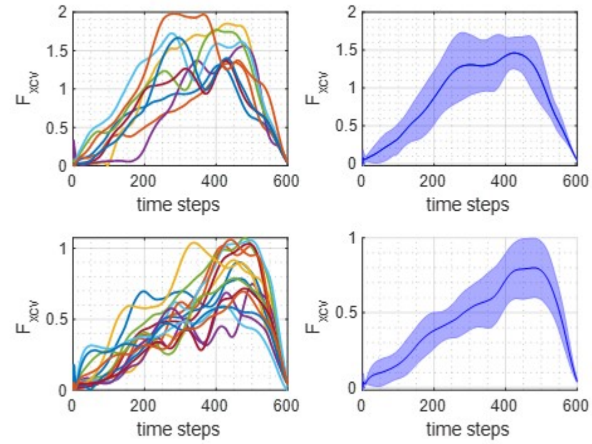

Fig. 8: Raw external force data from experts, resampling data,mean and variance between each data during excavation. Top: flat terrain, bottom: slope terrain

A. Expert Force Trajectory

The external contact force data from experts acquired consecutive three times digging on the flat and the two types of slopes. We conduct a resample process and analyze the excavation force of experts in normalized dimensionless quantity, which is defined as F_{xcv}=$\|F_x^2 + F_z^2\|/k$ with normalized factor k. The noticeable feature of the expert force trajectory is the trapezoid pattern maintaining constant force as threshold in Fig. 8. The contact force threshold shows E$(F_{xcv,flat}) = 1.62$, $\sigma(F_{xcv,flat}) = 0.24$ in flat terrain , and E$(F_{xcv,slope}) = 0.86$, $\sigma(F_{xcv,slope}) = 0.43$ in slope.

B. Online Trajectory Modulation

We implement the coupling movement primitive in Sec. II-C to modulate the trajectory online based on excavation force. We assume that the excavation force decreases when the excavation trajectory changes shallower perpendicular to the ground. To satisfy invariance property in DMP, we set the DMP coordinate that has the first coordinate as the line of the initial and the goal position and the second coordinate is perpendicular to the first coordinate. Fig. 9 shows that the modulating force $C \in \mathbb{R}^2$ perpendicular to the ground and divided C_x and C_y along the DMP coordinate (x_{DMP}, y_{DMP}). Under the assumptions, the following coupling movement primitive is formulated with $w = F_{xcv} - F_{threshold}$ as

$$\tau\dot{z} = \alpha_p(\beta_p(g-y)-z) + f(T,s) + c_2\dot{C}_{DMP} \quad (10)$$

$$\tau\dot{y} = z + c_1 C_{DMP} \quad (11)$$

$$C(s) = \begin{cases} w & \text{if } w > 0 \\ 0 & \text{otherwise} \end{cases} \quad (12)$$

$$C_{DMP}(s) = \begin{bmatrix} C_x \\ C_y \end{bmatrix} = \begin{bmatrix} -C(s)\sin(\theta_{DMP} - \theta_{slope}) \\ C(s)\cos(\theta_{DMP} - \theta_{slope}) \end{bmatrix} \quad (13)$$

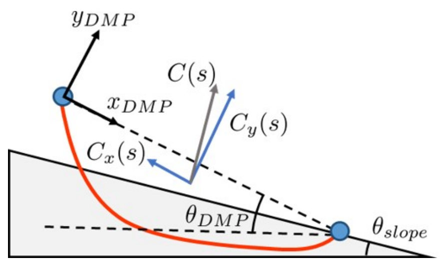

Fig. 9: Schematic of the coordinates of DMP dynamics and online modulation strategy.

with state vector $y \in \mathbb{R}^2$ is the p_x and p_y relative to DMP coordinate and $z \in \mathbb{R}^2$ is the velocity of the state. We consider only positive force feedback for excessive force respecting in (12).

V. Experiment

We evaluate the suggested algorithm with the customized Doosan DX380LC described in Sec. II-A. We conduct the three times consecutive digging in flat and two different angle of slopes. One slope angle is 26.05 degrees which is interpolated task parameter of training data and the other is 32.2862 degrees extrapolated task parameter. The generalization performance of the algorithm is verified through the interpolated and extrapolated task parameters.

The embedded PC for trajectory planning utilizes Intel i7 2.7GHz NUC and composed ubuntu-based ROS architecture. CAN communicates with the excavator in the 100Hz communication cycle, obtains the excavator configuration information and transmits the trajectory planning information in $\boldsymbol{q}$. LiDAR is connected to Nvidia Jetson TX2 and transmits PCD information to NUC PC in the 10Hz period. We set the threshold of the excavation force as $F_{th,slope}$=1.0 $\times$ 10^5N and $F_{th,flat}$=1.5 $\times$ 10^5N from experts force data. Hyper-parameters for coupling movement primitives are assigned as α_p=5.0, β_p= $\sqrt{20}$, c_1=0.03, and c_2=0.008.

A. Experimental Results

The planned trajectories in the flat terrain are shown in Fig. 10. As shown in the figure, it adapts to changes of the depth from the consecutive excavations and properly generates deeper trajectories in series. Fig. 11 shows that the force trajectory in flat terrain has a trapezoidal pattern similar to the expert pattern that maintains a constant force at the maximum. In the flat terrain, the excavation force F_{xcv} is under the threshold, so the algorithm plans the trajectory without online modulation for excessive excavation force. Weighing after digging measured with a momentum based observer marks 3.03 tons, 89.9% of the full bucket, and it indicates sufficient performance in terms of productivity.

The nominal and modulated trajectory for the slope is shown in Fig. 12. The blue dotted lines are the nominal trajectories from the extracted task parameters and the red solid lines are the modulated trajectories based on the estimated excavation force. Comparing with the red plot in Fig. 13, excavation forces exceed above the threshold at the first

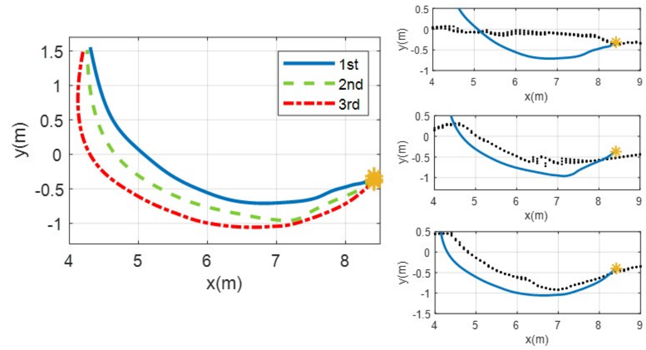

Fig. 10: Results of digging in flat terrain- left: plot of the three trajectories which operates deeper, right: each trajectory with y-dir flatten PCD before digging. The initial point is a yellow star.

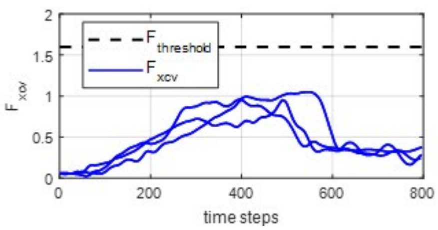

Fig. 11: External force data F_{xcv} during digging in flat terrain.

and second digging in both terrains, and the trajectories are modulated to the shallower direction than nominal.

Moreover, Fig. 13 highlights the performance of force feedback modulation compared to the nominal trajectory. Modulated red plots have a trapezoidal pattern with a similar tendency to expert force trajectory, while the nominal trajectories have a pattern that peaks at much higher excavation forces above the threshold. The maximum excavation forces of nominal trajectories are 1.68 and 1.93 in each slope, and that of modulated trajectory are 1.25 and 1.38. Accumulated error for the force above the threshold from the nominal trajectory shows 1.72 and 2.40 times greater in each slope. This result shows that the suggested algorithm prevents problems such as overturning due to excessive excavation force and enables to emulate the optimal force pattern similar to the expert.

VI. Conclusion

In this paper, we propose a novel excavation trajectory planning algorithm, which can effectively learn and retrieve the expert's kinematic and dynamic strategy. The algorithm learns the expert position trajectories interacting with complex soil model through DMP via neural network structure, so guarantees safety and robustness. Also, online trajectory modulation based on the estimated excavation force prevents excessive deep excavation and adapts to changes in the dynamic properties of the ground. We implement our approach to customized excavator and evaluate in the flat and slope terrains. Experimental results show that the suggested

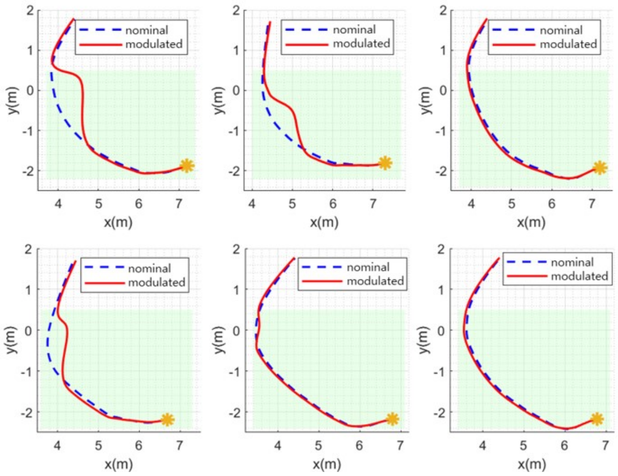

Fig. 12: Nominal trajectories and online modulating trajectories in slope 1 (top) and slope 2 (bottom) for consecutive three times excavations. The green area is digging inside the ground and the rest is booming up to designated goal point. The initial point is a yellow star.

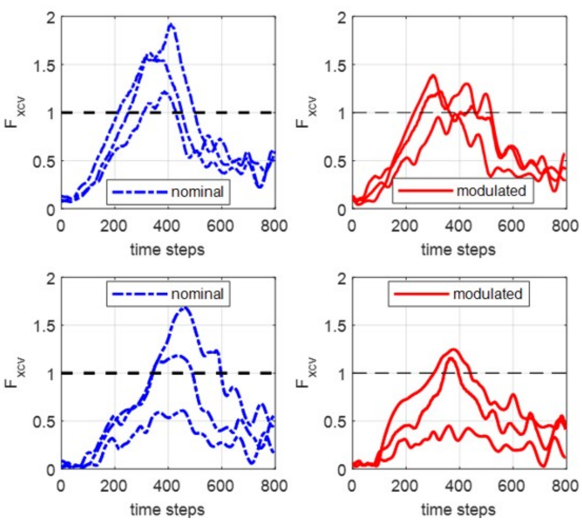

Fig. 13: External force results on slopes. The blue dotted lines are the results of the excavation force without feedback, and red lines are the excavation force results of considering coupling feedback. (top) slope 1, (bottom) slope 2.

algorithm can generate the trajectory which follows the both expert's position and force trajectory with generalization performance ensuring sufficient excavation weighing. The possible next step for this work is to develop an algorithm to find the optimal coupling gain suitable for the excavator system and improve the performance from the extrapolated task parameters.

REFERENCES

[1] L. E. Bernold, "Motion and path control for robotic excavation," *Journal of Aerospace Engineering*, vol. 6, no. 1, pp. 1–18, 1993.

[2] F. SCHREIBER, P. RAUSCH, and M. DIEGELMANN, "Use of a machine control & guidance system, determination of excavator performance, cost calculation and protection against damaging of pipes and cables," in *1st International Conference on Machine Control & Guidance*, 2008, pp. 1–10.

[3] Y. Shimano, Y. Kami, and K. Shimokaze, "Development of pc210lci-10/pc200i-10 machine control hydraulic excavator," *Komatsu technical report*, vol. 60, no. 167, 2014.

[4] "New cat automated grade controls usher in more efficient excavators," https://bit.ly/38eqMeY, Nov 2015, accessed on 2020-02-29.

[5] "Leica geosystems for an excavators," https://bit.ly/32FmtIJ, accessed on 2020-02-29.

[6] Y. Yang, L. Zhang, X. Cheng, J. Pan, and R. Yang, "Compact reachability map for excavator motion planning," in *2019 IEEE/RSJ International Conference on Intelligent Robots and Systems (IROS)*, Nov 2019, pp. 2308–2313.

[7] S. Sing, "Synthesis of tactical plans for robotic excavation," Ph.D. dissertation, Carnegie Mellon University, 1995.

[8] S. Lee, D. Hong, H. Park, and J. Bae, "Optimal path generation for excavator with neural networks based soil models," in *2008 IEEE International Conference on Multisensor Fusion and Integration for Intelligent Systems*. IEEE, 2008, pp. 632–637.

[9] F. E. Sotiropoulos and H. H. Asada, "A model-free extremum-seeking approach to autonomous excavator control based on output power maximization," *IEEE Robotics and Automation Letters*, vol. 4, no. 2, pp. 1005–1012, 2019.

[10] D. Jud, G. Hottiger, P. Leemann, and M. Hutter, "Planning and control for autonomous excavation," *IEEE Robotics and Automation Letters*, vol. 2, no. 4, pp. 2151–2158, 2017.

[11] D. Jud, P. Leemann, S. Kerscher, and M. Hutter, "Autonomous free-form trenching using a walking excavator," *IEEE Robotics and Automation Letters*, vol. 4, no. 4, pp. 3208–3215, 2019.

[12] S. Schaal, "Dynamic movement primitives-a framework for motor control in humans and humanoid robotics," in *Adaptive motion of animals and machines*. Springer, 2006, pp. 261–280.

[13] I. Goodfellow, Y. Bengio, and A. Courville, *Deep learning*. MIT press, 2016.

[14] D. I. Europe, "Doosan concept-x," https://youtu.be/vQkTJjrnmDc, Nov 2019, accessed on 2020-02-29.

[15] "Concept-x introduced by doosan infracore," https://www.equipmentjournal.com/tech-news/doosan-infracore-concept-x-automation/, Nov 2019, accessed on 2020-02-29.

[16] K. Kim, M. Kim, D. Kim, and D. Lee, "Modeling and velocity-field control of autonomous excavator with main control valve," *Automatica*, vol. 104, pp. 67–81, 2019.

[17] A. J. Ijspeert, J. Nakanishi, H. Hoffmann, P. Pastor, and S. Schaal, "Dynamical movement primitives: learning attractor models for motor behaviors," *Neural computation*, vol. 25, no. 2, pp. 328–373, 2013.

[18] A. Gams, A. J. Ijspeert, S. Schaal, and J. Lenarčič, "On-line learning and modulation of periodic movements with nonlinear dynamical systems," *Autonomous robots*, vol. 27, no. 1, pp. 3–23, 2009.

[19] A. Gams, B. Nemec, A. J. Ijspeert, and A. Ude, "Coupling movement primitives: Interaction with the environment and bimanual tasks," *IEEE Transactions on Robotics*, vol. 30, no. 4, pp. 816–830, 2014.

[20] S. Haddadin, A. De Luca, and A. Albu-Schäffer, "Robot collisions: A survey on detection, isolation, and identification," *IEEE Transactions on Robotics*, vol. 33, no. 6, pp. 1292–1312, 2017.

[21] S. Levine, C. Finn, T. Darrell, and P. Abbeel, "End-to-end training of deep visuomotor policies," *The Journal of Machine Learning Research*, vol. 17, no. 1, pp. 1334–1373, 2016.